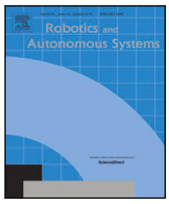
Robotics and Autonomous Systems 184 (2025) 104863



Contents lists available at ScienceDirect

Robotics and Autonomous Systems

journal homepage: www.elsevier.com/locate/robot





Automatic control for swing-free control of suctioned products in robotic pick-and-place operations

R.J. van der Kruk [a,*], B.H.T. Bindels [a], H.P.J. Bruyninckx [a,b,c], M.J.G. van de Molengraft [a]

[a] Control Systems Technology, Faculty of Mechanical Engineering, University of Technology Eindhoven, P.O. Box 513, Eindhoven, 5600 MD, The Netherlands
[b] Department of Mechanical Engineering, K.U. Leuven, Celestijnenlaan 300, Leuven, Postbus 2420 3001, Belgium
[c] Flanders Make Leuven, Gaston Geenslaan 8, 3001 Heverlee, Belgium

ARTICLE INFO

Keywords:
Self tuning
Vibration reduction
Swing-free
Robotic pick-and-place
Input shaping
Vacuum gripper

ABSTRACT

This paper introduces a new control method for suctioned products in robotic pick-and-place applications with the aim of significantly reducing the peel-off force and overshooting. A controlled cart-pendulum-mass model approximates the complex dynamics of the robot with the attached load. A design procedure is outlined based on the relationship between relative dynamic placement inaccuracy and the ratio of vibration time to move time. An algorithm is outlined for the implementation of the design method. This procedure enables the determination of the highest acceleration value that maintains accuracy within the desired range. This paper builds on previously published conference work (van der Kruk et al., 2023), incorporating a self-adjusting method, a specialised gripper, validation for significant mass variations, a frequency domain analysis and experimental results using chicken fillets handling. A passive rotational single degree of freedom is incorporated into a standard bellow vacuum gripper to minimise the torque applied to the end effector alongside input shaping. The accelerations allowed in the end effector are increased. Robustness against peel-off at higher accelerations is improved while leveraging the advantages of swing-free controls. Automatic tuning of the control parameters is achieved through a background subtraction method that measures the tracking errors in the joint motion controllers. The effectiveness of the proposed method is validated through a practical use case involving chicken fillet packaging with a fast industrial delta robot. This is a weight and pick-up spread case test. All fillets in the industrial use-case weight distribution range can be consistently picked and handled using the same constant parameters without experiencing peel-off. The Zero Vibration input shaper demonstrates the best overall performance for realistic variations (such as weight and pick-up pose), well within 10% of the variations of the natural frequency.

1. Introduction

1.1. Background

In food processing, the scarcity of skilled personnel, along with considerations of efficiency and hygiene, constitutes the main drivers for replacing human labour with industrial robots. However, current robot technology faces challenges in adequately handling variations, such as those in size and weight, as exemplified in Fig. Fig. 1. In this illustration, the fillet products are autonomously selected and picked from a conveyor belt and placed on trays Fig. 2 using delta robots, equipped with enclosure grippers, which fold the sides of the chicken fillet underneath, creating a convex shape to mechanically restrict the movement of the fillet. Robotic grippers are designed to offer high flexibility and multifunctionality [1,2].

The economic value of improving performance through swing-free motions is substantial, given that the annual count of robotic picks in food packaging is estimated at 2.5×10^{12}, with more than 90,000 robots deployed worldwide [3]. In a case study, we [4] demonstrated a 50% reduction in the net movement time for the placement of a packed load of mozzarella using a suction cup gripper. This reduction suggests that the productivity of an existing packaging line, equipped with multiple robots, could improve by several tens of percent. An alternative to the enclosure gripper is the flexible and easily manufacturable vacuum gripper. However, a significant drawback of this gripper is that when the product is suctioned and moved rapidly, it tends to swing, which leads to additional time needed for placement and the risk of the product peeling off. In this paper, our focus is on exploring ways to minimise the overall settling time without experiencing swinging or peeling off, even when the properties of the product are unknown.

* Corresponding author.
E-mail address: r.j.v.d.kruk@tue.nl (R.J. van der Kruk).

https://doi.org/10.1016/j.robot.2024.104863
Received 26 July 2024; Received in revised form 29 October 2024; Accepted 9 November 2024
Available online 16 November 2024
0921-8890/© 2024 The Authors. Published by Elsevier B.V. This is an open access article under the CC BY license (http://creativecommons.org/licenses/by/4.0/).

Nomenclature

abbreviation	explanation for the abbreviation
ω_n	Natural vibration frequency [rad/s]
τ	Dimensionless vibration time [–]
θ	Angle of product suspended to robots end effector [rad]
ζ	Damping ratio [–]
A_i	impulse Amplitude of input shaper [–]
r	Reference, trajectory displacement [m]
T_{acc}	Acceleration time in trajectory [m/s^2]
T_d	Damped vibration time [s]
T_j	Jerk time, the duration of jerk [s]
T_m	Move time, the total acceleration and deceleration time [s]
T_s	Sample time [s]
u_0	Relative overshoot [–]
V_{tol}	Tolerance level for EI input shaper [%]
z	Forward shift operator
l	Equivalent length of load [m]

1.2. Literature overview

The topic of swing-free handling of objects by robots has received limited attention in scientific research articles in recent years. The classical work of Starr [5] discussed methods for determining specific motion trajectories that allow suspended objects to come to a stop at the desired end position. While proper programming of acceleration and deceleration based on the vibration time of the suspended product is emphasised, these methods lack robustness and are specific to the product in question.

The topic of swinging products is related to the swing-up control of an inverted pendulum on a cart [7,8], where swing-free point-to-point control of underactuated systems is achieved using a two-degrees-of-freedom control method with a nonlinear feedforward position controller, an optimal feedback controller and trajectory design. The challenge lies in designing an appropriate feedforward controller, as demonstrated by swing-free experimental results; see [9], where energy control was used, highlighting the critical dependence on the maximum acceleration of the pivot.

Input shaping is a method to create motion trajectories to effectively reduce transient oscillations in flexible systems induced by the reference. The classical zero vibration (ZV) input shaper [10] provides a way to suppress the transient oscillation in a lightly-damped oscillatory feedback system by shaping the spectral content of the motion profile by means of time-delay filters.

Despite the potential benefits, input shaping techniques are often mistakenly considered suitable only for open-loop systems. A significant knowledge gap exists in the industrial applications of input shaping for lightly damped mechatronic systems. Misunderstandings of implementation aspects have led to limited applications in robotic systems, where a shaped reference trajectory could reduce the overall move time of suspended objects, as reported in [11]. For the control of cranes, the benefits of input shaping are well known; see [12]. Although the input shaper framework was created in the early 1990s by [10], still nearly 100 scientific publications appeared in the last decade related to practical applications and optimisation of cranes; see [13–18]. However, input shaper applications for swing-free control of suctioned objects remain rather limited, and there is a lack of literature that clearly describes its application and the potential improvements that could be attained in this field.

Conventionally designed frequency domain filters, such as notch and low-pass filters, are never better than the mentioned input shapers, as proved in [19]: A causal real-time filter distorts the phase of the resulting signal and penalties such as ringing or long move time occur. Many robust input shapers have been reported in literature and typically have a longer move time, leading to a slow response. The balance between vibration reduction, trajectory move time, and robustness against vibration variations is not fully described and may be specific to applications. The automatic tuning by iterative learning control for point-to-point motions using combined reference shaping and feedforward is described in [20]. However, their shaping is based on polynomial basic functions and does not reduce the transient oscillations. Van der Kruk et al. [4] detail experimental results on minimising the vibrations of mozzarella cheese immersed in a liquid within a bag attached to a robot's end effector, demonstrated via a copy spread test. This paper builds upon that work, exploring its application to a weight and pick-up pose spread use case test with chicken fillets. The application of input shaping described in this paper yields non-zero but low levels of swing. Many researchers have traditionally examined transient oscillation in the frequency domain, assuming that system inputs are one cycle of a repeating waveform. We adopt a time domain approach, with frequency domain views primarily for comparison, as in [21].



Fig. 1. Robobatcher a delta robot line to pick-and-place fillets from a conveyor belt to a tray. *Source:* Marel [6].

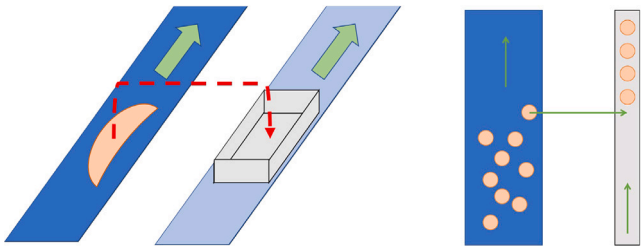


Fig. 2. Typical pick-and-place paths.
Source: Marel [6].

1.3. Main contribution of this paper

This paper introduces and validates a self-tuning control method designed for robotic systems, aiming to satisfy the requirement of overshoot while minimising the overall motion time for pick-and-place movements of suctioned products. An algorithm is given for implementation of the design method for trajectories and shaper. In addition, to prevent peel-off and swing-free traction controls, a rotational degree of freedom is incorporated into the vacuum gripper. The gripper used in the experiments is a hinge gripper with a single suction cup which results of 40 percent higher peel-off torque. All other simulation results use the controlled mass-cart-pendulum model which represents both the suction cup and the hinge gripper for displacements of the load. This makes handling non-rigid food products which vary in size and weight possible. A frequency domain view of trajectory generation and input shaping is presented.

1.4. Organisation of this paper

This paper is organised as follows. In Section 2 trajectory generation and input shaping are revisited. A model for predicting the dynamical behaviour of swinging objects is demonstrated in Section 3. Section 4 describes the control method. In Section 5 the experimental results are presented and discussed. Section 6 describes the self-tuning control method. Finally, in Section 7, the conclusion follows.

2. Preliminaries

2.1. Trajectory generation

To execute motion tasks, trajectories need to be generated to interpolate waypoints towards the endpoint. As a result, real-time trajectory generation calculates a trajectory $r(t)$ to prevent actuator saturation considering constraints such as maximum acceleration, speed, and workspace [22]. We disregard the constant-velocity phase as it does not influence the dynamics and is not achieved during rapid pick-and-place operations. The acceleration time history of the trajectory, the forcing function, will determine the transient response. The move time, the total acceleration and deceleration time, T_m are usually assumed to be long relative to the first natural period of damped vibration T_d. We use the definition of τ as the dimensionless vibration time.

$$\tau = \frac{T_d}{T_m}. \tag{1}$$

Here T_m is the shaped reference move time. The black curves in Fig. 3 illustrate point-to-point trajectories over a single distance, transitioning from rest to rest. The position trajectory $r(t)$ forms an S shape and follows a parabolic path, the velocity profile $v(t)$ is triangular, and the acceleration trajectory $a(t)$ features both a positive and a negative pulse. This can be represented by:

$$\ddot{r}(t) = a(t) = a_{max} \int_{-\infty}^{t} (\delta(\tau) - 2\delta(\tau - T_{acc}) + \delta(\tau - 2T_{acc}))\, d\tau. \tag{2}$$

A Jerk Limited (JL) profile produces a smooth trajectory as illustrated in Fig. 3, but it also leads to a higher peak acceleration, which results in greater deformation and consequently higher transient oscillations. The JL trajectory, sometimes named double S, is frequently used and is available in most industrial digital servo controllers. The quintic polynomial trajectory [22] has no discontinuities in acceleration and can be compared to the JL and cycloid when used for point-to-point trajectories.

In the sequel, we consider only a displacement reference, and its derivatives are not used or needed. The sole preconditions are the position set points at specific times. These could be pre-programmed or generated in real time from camera devices.

2.2. Trajectory input shaping

In addition to high-order trajectories, input shaping is a technique to generate signals that avoid exciting vibration modes while the final position is reached. Due to its advantages, such as simplicity and effectiveness, it has received much attention in control theory. The impulse response of input shapers in the time domain is the following.

$$f(t) = \sum_{i=1}^{n} A_i \delta(t - t_i), \qquad \sum_{i=1}^{n} A_i = 1, \quad t_1 = 0. \tag{3}$$

where A_i is the amplitude of the ith impulse, t_i is the applied time moment of the ith impulse. δ is the unit impulse or the Dirac function. The shaped response $r_s(t)$ of the trajectory $r(t)$ to the impulses of the input shaper $f(t)$ is equal to

$$r_s(t) = \int_{-\infty}^{\infty} f(t - \tau) r(\tau)\, d\tau = f(t) * r(t) \tag{4}$$

by convolution. The constraints imposed to the Zero Vibration (ZV) input shaper [23] are achieving zero vibration and minimising delay at the modelling frequency. The parameter settings for all shapers require the natural vibration frequency ω_n and the damping ratio ζ. With

$$k = e^{-\zeta\pi/\sqrt{1-\zeta^2}}, \qquad T_d = 2\pi/\omega_n\sqrt{1-\zeta^2}. \tag{5}$$

The ZV impulse response is

$$f_{ZV}(t) = \frac{1}{1+k}\delta(t) + \frac{k}{1+k}\delta(t - T_d/2). \tag{6}$$

The Extra Insensitive (EI) shaper [24,25] does not attempt to force the vibration to zero. A small level of vibration V_{tol} is allowed at the modelled frequency and the robustness against modelling frequency errors is enhanced. The impulse response of the EI shaper is

$$f_{EI}(t) = k_1\delta(t) + (1 - k_1 - k_3)\delta(t - T_d/2) + k_3\delta(t - T_d). \tag{7}$$

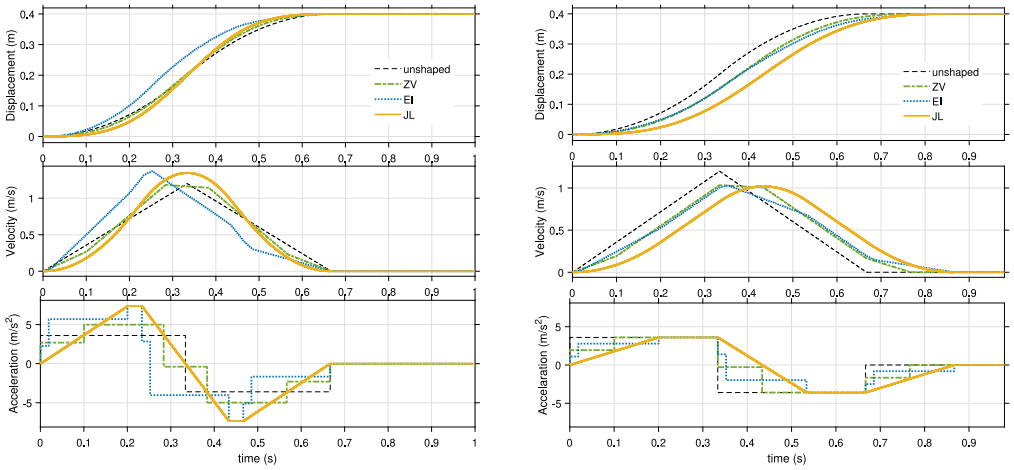
The parameters of the undamped (without viscous friction) EI shaper [26] are

$$k_1 = k_3 = (1 + V_{tol})/4, \tag{8}$$

Typically $V_{tol} = 5\%$. The duration of the EI shaper equals that of the ZVD (Zero Vibration Derivative) shaper, one damped cycle of the vibration, but EI is considerably more robust. The input shaping of the parabolic results in pulsed acceleration profiles for ZV and EI as depicted in Fig. 3. This differs from the linear acceleration profile of the JL profile, which is usually generated directly as a third-order piecewise spline profile. Alternatively, it can be realised as an input shaper, a finite impulse response (FIR) filter applied to the parabolic trajectory.

$$f_{JL}(t) = \frac{1}{T_j}\int_{-\infty}^{t} (\delta(t) - \delta(t - T_j))\, d\tau, \quad T_j = T_d \tag{9}$$

Here, the value of the jerk is $1/T_j$. The shaped trajectories increase the move time T_m, which consequently affects the value of τ. These relationships are presented in Table 1. A comparison of equal move times τ and equal acceleration input shaping is shown in Fig. 3. In swinging object applications, the maximum acceleration is determined by the object and its gripping rather than by the robot. We are striving



(a) Trajectories with equal move time. The shaped trajectories exhibit 50% (ZV) and 100% (EI,JL) higher acceleration compared to the unshaped trajectory.

(b) Trajectories with equal acceleration. Trajectories with shaping demonstrate a move time that is 0.1 seconds longer for ZV and 0.2 seconds longer for EI and JL than those without shaping.

Fig. 3. Comparison of parabolic trajectories with and without the shaping of the ZV, EI, and JL input shapers. $\tau = 0.3$.

Table 1
Shaped and unshaped parabolic trajectories and their relation to shaped move time T_m and the dimensionless vibration time τ. T_d: damped natural vibration time, T_{acc}: acceleration time.

Parabolic trajectory	Shaped move time T_m	τ
Unshaped	$2T_{acc}$	$T_d/(2T_{acc})$
ZV shaped	$2T_{acc} + T_d/2$	$T_d/(2T_{acc} + T_d/2)$
EI, JL shaped	$2T_{acc} + T_d$	$T_d/(2T_{acc} + T_d)$

for a control method to reduce oscillations with input shapers, where we prescribe the move time; see Fig. 3a.

The sampling interval for digital input shaper schemes must be a fraction of the damped natural vibration period T_d. If the oversampling rate is equal to 100 $T_s = T_d/100$, the transfer functions $F(z)$ of the input shapers in the z-domain are;

$$F_{ZV}(z) = \frac{1}{k+1}\frac{z^{50}+k}{z^{50}}, \tag{10}$$

$$F_{EI}(z) = \frac{k_1 z^{100} + (1-k_1-k_3)z^{50} + k_3}{z^{100}}, \tag{11}$$

$$F_{JL}(z) = \frac{1}{T_j}\frac{z}{z-1}\frac{(z^{100}-1)}{z^{100}} \tag{12}$$

Here, z is the forward pulse shift operator. These time delay transfer functions are different from conventional signal processing filters. The ZV shaper has 50 poles in at $z = 0$ and the same number of zeros distributed at an equal distance over the unit circle.

When using input shaping, there are two key trade-offs: move time and parameter robustness; see, e.g. [25]. To solve these problems, learning input shapers and adaptive input shapers were developed [27]. Even trajectory compression and reconstruction were proposed [28]. The disadvantages of these methods are complexity and the usage of higher acceleration. At equal maximum acceleration they are never shorter than the trajectory design method proposed in this paper. Typically, in industrial applications where time response is a priority, ZV and EI shapers are used [29]. The ZV shaper provides the quickest time response, while the EI shaper offers superior robustness against model inaccuracies.

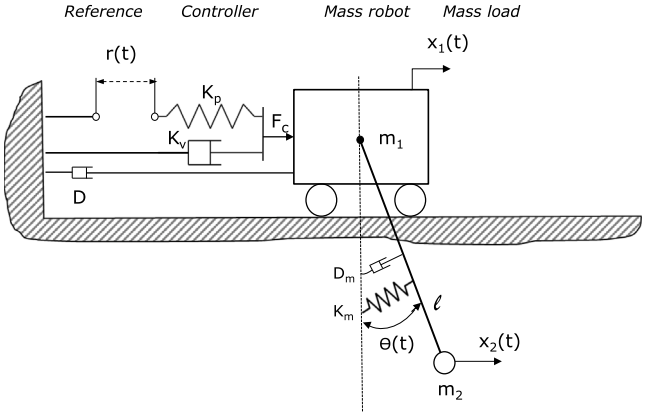


Fig. 4. Abstracting the manipulation of a swinging item picked up by a suction cup: A two-dimensional pendulum model suspended and guided by a position-controlled cart.

3. Modelling method of a swinging product suspended by a robotic suction system.

The product gripped by a vacuum under a robot end-effector can be modelled as a controlled cart-pendulum-mass system as shown in [4]. It involves a position-controlled cart that transports a load suspended by a pendulum, as illustrated in Fig. 4. The model has two degrees of freedom: the horizontal position x_1 of the cart and the rotation θ of the load in the vertical plane.

The horizontal movement of the load x_2 is observed. The movement of the cart $x_1(t)$ is measured by the joint position encoders. The robot mechanism is considered as a rigid body, since the joint controllers of the robot are typically tuned for a fast and accurate response with high servo stiffness of the end effector, resulting in a bandwidth significantly higher than the vibration frequency of the load. This mass-cart-pendulum system is an underactuated system: the number of actuators (one) is less than the degree of freedom (two) of the system. Mechanical parameters are given in [4].

The equations of motion are given in Eqs. (13), (14), (15), and (16) see [4].

$$F_c = (m_1+m_2)\ddot{x_1} + m_2 l\ddot{\theta}\cos(\theta) - m_2 l\dot{\theta}^2\sin(\theta) + D\dot{x_1} \tag{13}$$

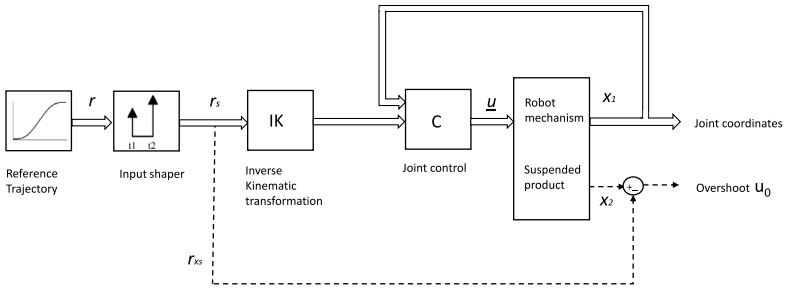


Fig. 5. Control system for a delta robot with three joints. The inverse kinematic (IK) transformation and the generation of the reference trajectory are executed in the 3D task space. The dashed line signifies that the performance output x_2 is not directly measured during operation.

$$m_2 l\ddot{x}_1 \cos(\theta) + m_2 l^2\ddot{\theta} + D_m\dot{\theta} + m_2 lg \sin(\theta) + K_m\theta = 0 \tag{14}$$

$$x_2 = x_1 + l \sin(\theta) \tag{15}$$

$$F_c = K_p(r - x_1) - K_v\dot{x}_1. \tag{16}$$

The control input for the cart is represented by the driving force F_c. The joint position controllers in the horizontal direction are described by equation $F_c = K_p(r-x_1)-K_v\dot{x}_1$. Food packages and fillets are considered point masses, with the assumption that the stiffness and damping of the gripper are lower than those attributes in the loaded product, as validated in [4]. Expressed in a generalised vector format, the equations of motion are given by

$$M(q)\ddot{q} + C(q,\dot{q})\dot{q} + D\dot{q} + g(q) = F_c \tag{17}$$

with the positive definite mass matrix M, the Coriolis matrix C, the damping matrix D, the vector of gravity g and the control force F_c. The variables q are generalised coordinates that are mutually independent, each depending on time.

The significance of this controlled cart-mass-pendulum model lies in the derivation of the relative dynamic inaccuracy u_0 for point-to-point tasks based on the ratio τ of the damped vibration time to move time T_d/T_m.

Simulations of the responses of the load position were collected for parabolic and input-shaped parabolic trajectories. No further simplification or linearisation is carried out to avoid reduced accuracy. The control force calculations are executed in a time-discrete way, including a zero-order hold with a sample rate far beyond the bandwidths of the joint angle control loop.

4. Control means and methods

The control method in this paper is based on the work of [4], but we provide a more comprehensive and detailed description. The 3D control scheme in Fig. 5 depicts the pose of the product, x_2, which needs to be controlled and is not directly measured but estimated from x_1 the robot actuator positions during operation when tuned. The actuator positions are used as feedback signals. This type of control is inferential; see [30,31]: the primary performance measurement is not available for control and is estimated from a secondary measurement. The robot joint feedback loops serve as subordinate controllers (C) and eliminate disturbances such as load changes and friction.

The reference trajectory defines the 3D path of the end effector x_1. Given that our primary concern is vibration in the pick-and-place direction, the other task space coordinates are synchronised, taking into account that the flexible design of the vacuum gripper does not restrict movement in other directions. Only for initialisation purposes, a sensor tag is attached to the product to measure x_2 and shape the controller. See 12, right picture with tag on the Mozzarella product package. The control during this research is in three dimensions, and the measurement of the vibration is in one dimension; along the vector of product transfer.

We use the definition of transient oscillation as the relative dynamic positioning inaccuracy u_0

$$u_0 = \frac{\max|r - x_2(t)|}{r}, \quad t > T_m \tag{18}$$

$x_2(t)$ is the position of the object to be handled. r is the reference end position. T_m is the shaped move time. Table 1 lists these values τ for the input shaper types. The expression $ml\ddot{x}_1\cos(\theta)$ in Eq. (14) denotes the inertial torque exerted on the pendulum mass m_2, which typically peaks when the acceleration transitions to deceleration. Fig. 6 presents the simulated results for various relative dynamic placement inaccuracy values corresponding to different values of τ. The overshoot is constrained by the length l. In unit fractions of T_d/T_{acc} where $\tau = 1/2, 1/4, 1/6, ..$ the pendulum overshoot approaches zero. Due to the strong inertial coupling, the swing excited during the acceleration period is exactly cancelled during the deceleration period. [32] describe a generalised method for damped oscillation swing-free stops of suspended payloads achieved by arbitrary acceleration and deceleration timed to the natural frequency based on this principle. [33] describe this method for the swing-free transport of simply suspended objects that cannot be grasped by robot manipulators. Although this method is effective, it lacks robustness against changes in length (oscillation frequency).

In the range $\tau < 0.45$, the input shapers significantly reduce the overshoot compared to the unshaped parabolic trajectory. Here, the move time is larger than the vibration time, and only a low level of vibration is excited. This range is unsuitable for rapid pick-and-place operations. Within the interval $0.45 < \tau < 0.6$, the EI and JL input shapers do not help reduce the overshoot. However, the ZV input shaper significantly decreases the overshoot. For $\tau \gg 0.6$, the move time approaches the vibration period. The ZV input shaper significantly decreases the overshoot by a factor of 10 for $\tau < 0.8$. The EI and JL input shapers also reduce the overshoot, but not as effectively as the ZV shaper. Note that for values of $\tau > 0.5$, the shapers' profiles become dispersed as shown in 7d, resulting in a phase of low acceleration (constant velocity) between the pulses.

Fig. 8 displays the responses of the input shapers to demonstrate the overshoot in fast point-to-point tasks. The unshaped response exhibits minimal damping, leading to vibrations that almost match the length of the pendulum l, which is equivalent to the height of the suspended product. It is evident that the ZV shaper achieves the greatest reduction in overshoot. The impact of the relative inaccuracy of dynamic placement on the changes in the equivalent pendulum length l is described in [4]. When tuned, the ZV shaper exhibits the least overshoot for minor variations. Within the 10 percent range of length variations, the ZV shaper exhibits the highest suppression. This observation is consistent with findings in industrial overhead cranes [29], where it is observed that, except for the ZV input shaper, which not only decreases the cycle time but also reduces the oscillation in the load, all other

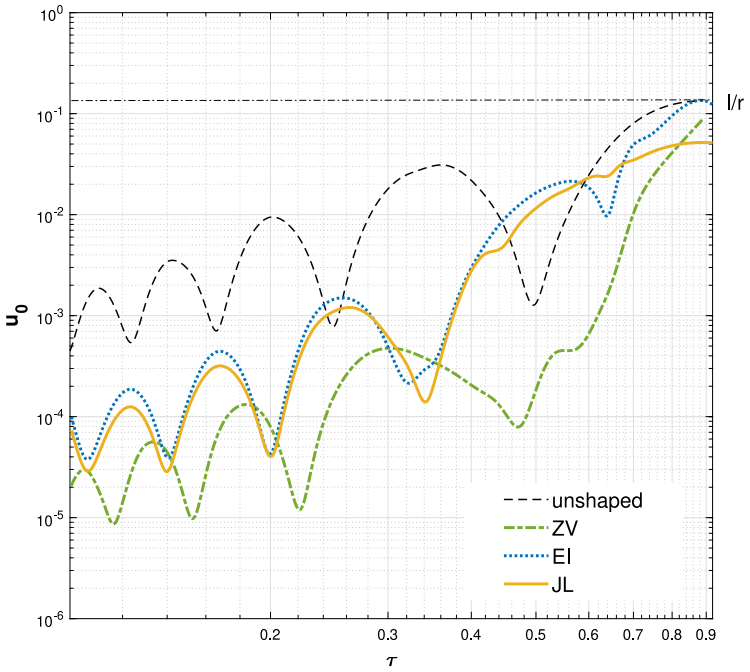


Fig. 6. Simulation results for the cart-pendulum-mass system: relative dynamic placement inaccuracy u_0 as a function of τ for shaped and unshaped parabolic trajectories; the damping offset (deviation from the model value) 10%.

input shaper algorithms lead to an increased production cycle time due to enhanced sway robustness. In the 10- to 20% range, the ZV shaper demonstrates the best performance when the bandwidths of the robot servo controllers are matched to the vibration frequency of the swinging product. The EI shaper provides improved robustness for even larger variations.

The significance of the relationship $u_0(\tau)$ lies in the fact that for a specified overshoot and vibration duration, a maximum value of τ is determined. The acceleration time T_{acc} can be selected to achieve τ using the values provided in Table 1 as described in Algorithm 1. This shows a design procedure for the input shaper parameters and the acceleration time T_{acc} of the parabolic trajectory. The peak acceleration varies and must be chosen to ensure that there are no swing moves.

Fig. 7 illustrates the various acceleration profile shapes as τ increases. The ZV and EI shapers produce asymmetric profiles, whereas the JL shaper maintains the symmetry of the initial profile. In Fig. 7d, the robust EI shaper amplifies the original acceleration by a factor of 7. By definition, the JL and EI shapers are not applicable to values $\tau \geq 1$.

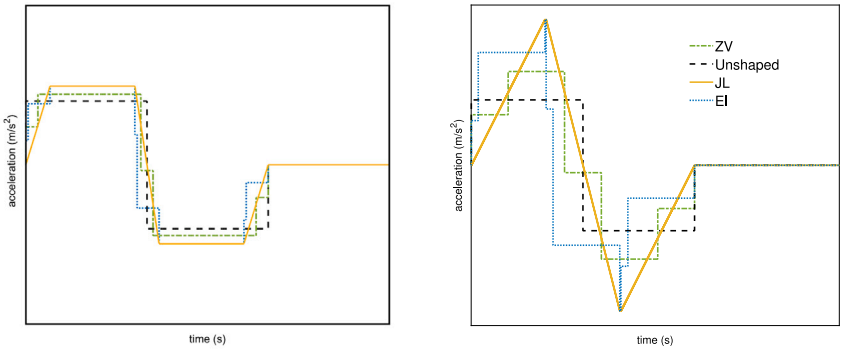
4.1. Frequency domain view

In Fig. 9 the frequency response of the transfer functions in Eqs. (10), (11) and (12) of these shapers are represented at low values of the damping ratio. The notch filtering of frequencies close to the natural frequency ω_n is depicted. Here, the phase shift is zero for all shapers. The Bode magnitude plot does not reveal that the shaping procedure results in an extension of the trajectory. In the Bode phase diagram this elongation is visible by the phase differences. The EI and JL input shapers exhibit a phase shift that is twice as large as that of the ZV input shaper. In the range of 10% natural frequency variations, the ZV input shaper suppresses the amplitude at the natural frequency in the reference by more than six times, despite being labelled the "least insensitive shaper". The EI shaper, while reducing the reference at a 10% frequency bias by more than 20 times, comes at the cost of a larger elongation of the move time. The JL input shaper is inferior to the EI

Algorithm 1 Design method for trajectory generator and input shapers

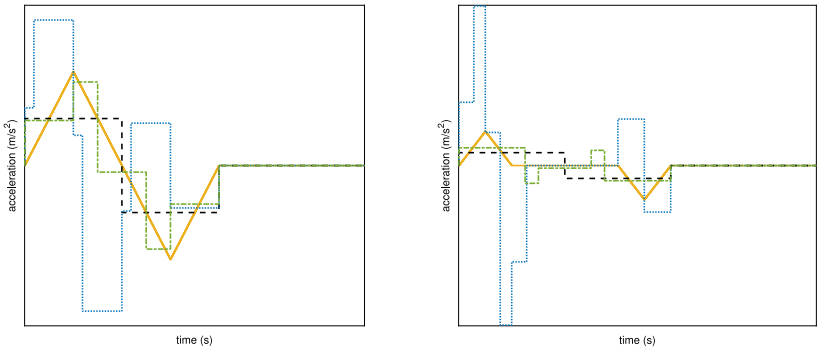
Require: $u_0(\tau)$ *relations*
Input: maximum overshoot specification U_0, displacement r, velocity v, natural frequency ω_n, damping ratio ζ, sample time T_s
Output: parameters trajectory T_{acc} and input shapers A_i, n_i

constant $V_{tol} = 0.05$;
$A_1 = 1; A_2 = 0; A_3 = 0; n_1 = 1; n_2 = 0; n_3 = 0$; {init}
$u_0 = U_0/r$;
$k = e^{\frac{-\zeta\pi}{\sqrt{1-\zeta^2}}}$; $T_d = \frac{\pi}{\omega_n\sqrt{1-\zeta^2}}$;
find τ and *shaper*; $T_m = T_d/\tau$; {*from* $u_0(\tau)$}
switch *shaper* **do**
  case 'ZV'
    $T_{acc} = ((T_m - T_d/2))/2$;
    $A_1 = 1/(1+k); A_2 = k/(k+1)$;
    $t_2 = T_d/2$; $n_2 = round(t_2/T_s)$;
  case '$ZV\&IM$'
    $T_{acc} = ((T_m - T_d))/2$;
    $A_1 = 1/(1+k); A_2 = k/(k+1)$;
    $t_2 = T_d/2$; $n_2 = round(t_2/T_s)$;
  case 'EI' {*undamped EI*}
    $T_{acc} = (T_m - T_d)/2$;
    $A_1 = (1+V_{tol})/4; A_3 = A1; A_2 = 1 - A_1 - A_3$;
    $t_2 = T_d/2$; $n_2 = round(t_2/T_s)$;
    $t_3 = T_d$; $n_3 = round(t_3/T_s)$;
  case 'JV'
    $T_{acc} = (T_m - T_d)/2; T_j = T_d$;
    $A_1 = 1/T_j; A_2 = -A_1$;
    $t_2 = T_j$; $n_2 = round(t_2/T_s)$;
  otherwise
  $T_{acc} = T_m/2$; {*Unknown shaper*}
endswitch



(a) $\tau = 1/10$. Slight increase in amplitude for the shaped profiles.

(b) $\tau = 1/3$. JL has no constant acceleration phase.



(c) $\tau = 1/2$. The amplitude of JL is less than that of EI.

(d) $\tau = 3/4$. The shaped profiles are dispersed over time. The amplitude of EI further increases

Fig. 7. The acceleration of the shaped trajectory profiles reveal a rise in acceleration with increasing τ values, assuming a constant move time. Notice that the EI shaper causes acceleration and deceleration twice for values of $\tau > 1/2$ and significantly exceeds the acceleration of the original parabolic.

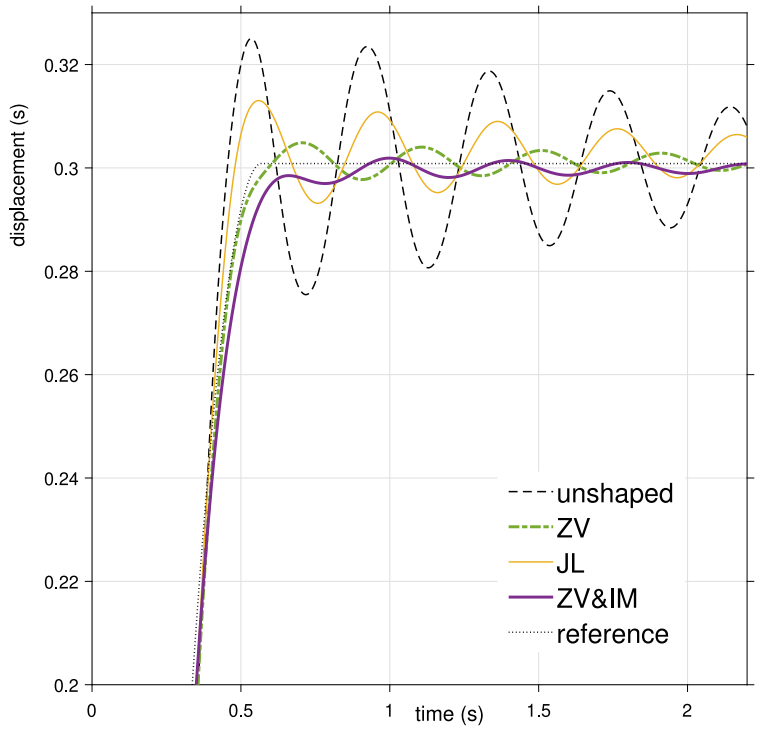


Fig. 8. Example of overshoot reduction by input shaping. Displacement responses for parabolic shaped 300 mm trajectories. Overshoot of unshaped parabolic is 25.4 mm. The reduction ratio using the input shapers is 9.4 (ZV), 8.8 (ZV robot bandwidth matched) and 2.7 (JL). The damping parameter mismatch is 10%. $\tau = 0.7$.

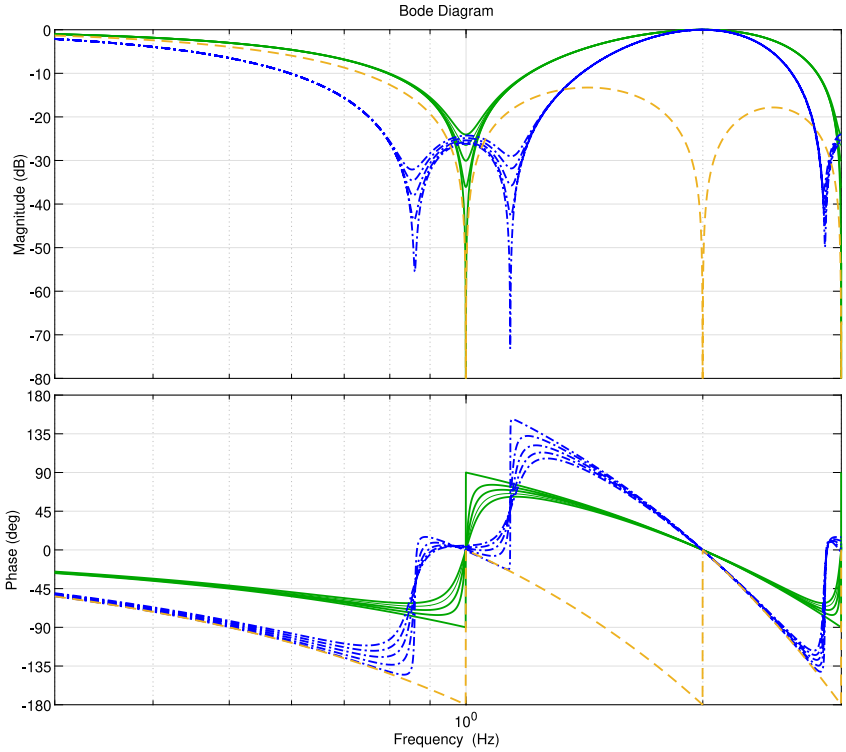


Fig. 9. Frequency response of the transfer functions (Bode plot) of the input shapers ZV (green), EI (blue, dash-dot) $V_{tol} = 1\%$ and JL (orange, dash). The natural frequency is 1 Hz, the damping ratios setting for ZV and EI are in range of 0, 1, 2, 3 4%.

shaper due to smaller insensitivity at an equal move time extension. It is also less effective for the ZV shaper due to a larger elongation of the move time, although it exhibits slightly better insensitivity. The JL shaper is frequently used, as it is available in industrial control packages. Its use is sometimes aimed at suppressing a range of high-frequency vibrations. However, this can be achieved more effectively by carefully selecting high-order low-pass filters in the feedback control loops. In such cases, all high-frequency disturbances are adequately suppressed.

The Laplace transform $a(s)$ of the acceleration profile $a(t)$ in Eq. (2) of the parabolic trajectory is

$$a(s) = \mathscr{L}\{a(t)\} = \int_{t=0}^{\infty} a(t)e^{-st}dt = \frac{a_{max}}{s}(1 - 2e^{-T_{acc}s} + e^{-2T_{acc}s}) \tag{19}$$

and the Laplace transform of the position reference profile $r(t)$ itself becomes

$$\mathscr{L}\{r(t)\} = \frac{a(s)}{s^2} = \frac{a_{max}}{s^3}(1 - 2e^{-T_{acc}s} + e^{-2T_{acc}s}) \tag{20}$$

Fig. 10 demonstrates the effect of input shaping in time and frequency domain. In the time domain, the pulsed acceleration trajectory of the parabolic trajectory is elongated with half of the vibration time. In the frequency response plots, the trajectory signals are filtered and suppressed towards zero at the resonance frequency of the swinging product at 2.5 Hz. At the frequency of $1/T_{acc}$ (3.5 Hz) the parabolic trajectory excitation is zero. Fig. 10(f) shows that the overshoot decreases from 30 mm to 1.7 mm, and the settling time, within a range of 5 mm, is reduced from 1 to 4 s. The overlap of the unshaped and shaped spectra is clearly influenced by the acceleration time ($\tau = 0.7$). The time and frequency response of a robotic swinging product in the horizontal pick-and-place direction is depicted in Figs. 10(d), 10(e) and 10(f). The ZV shaper effectively suppresses the swinging at 2.5 Hz. These data were acquired from a delta robot that grips a metal part with a vacuum gripper. Linearisation is achieved through parameter estimation to fit a linear model.

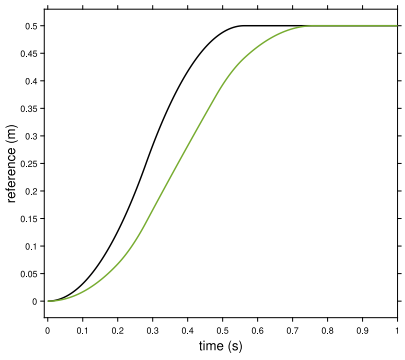
5. Experimental results for chicken fillet handling and discussion

5.1. Delta robot set up

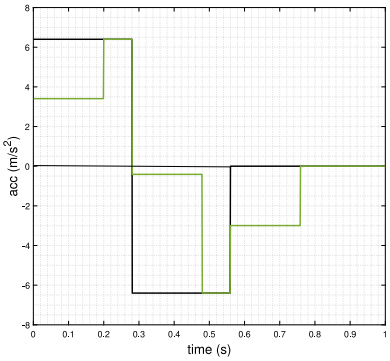
The industrial sdelta robot Spider depicted in Fig. 11 is used for the experiments. The DRP01, a parallel-structured robot, is driven by three rotary joints. Fig. 12 illustrates the mechanical structure of the Spider, with the physical parameters detailed in Table 2. It features three servo motors paired with planetary gearboxes, which are attached to the upper arms. The forearms consist of two parallel distal links connected to the upper arms via two spherical joints. The opposite ends of the distal links are connected to the travel platform using two spherical joints. This links the three forearms, forming a closed kinematic chain. It can move within Cartesian space, having three translational degrees of freedom (DOF) (x, y, z). An additional fourth servo motor is mounted on the travel platform to provide an extra rotational decoupled DOF along the z axis. The vacuum gripper end effector is attached to the motor shaft of the fourth joint. The working space is defined to avoid all singularities, resulting in a square cuboid space of 797 × 797 × 228 (W × L × H) [mm]. The delta robot operates as a purely translation mechanism, utilising both inverse and forward kinematic algorithms. It features two conveyors and a camera to represent an industrial state-of-the-practice food-packaging set-up. The open-control system features a real-time Beckhoff PLC Structured Text environment for actuators, sensors, and safety (TwinCat3). High-level control is enabled by interfaces such as Matlab/Simulink and Python. The lowest resonance frequency of the mechanism is in the range of 45 to 55 Hz.

The motor drive position error and control signal are accessible for real-time monitoring. In the development environment, features such as task space trajectories and inverse kinematics have been developed.

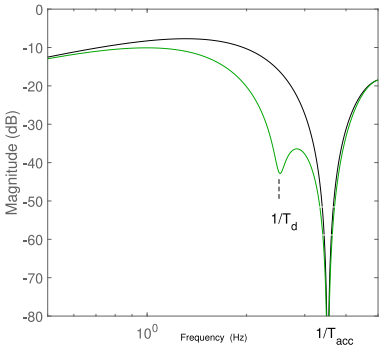
A video demonstration of the effect of input shaping for a pick-and-place task of packed chicken fillet is given in Fig. 13. Notice the large difference in vibration time during placement.



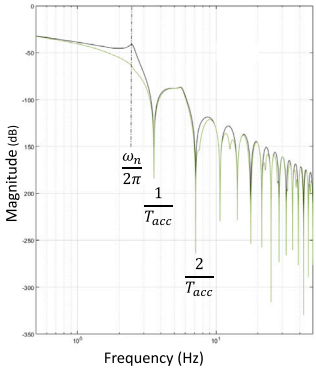
(a) Reference displacement $r(t)$



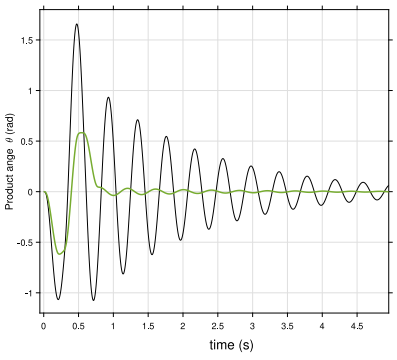
(b) Reference acceleration $\ddot{r}(t)$



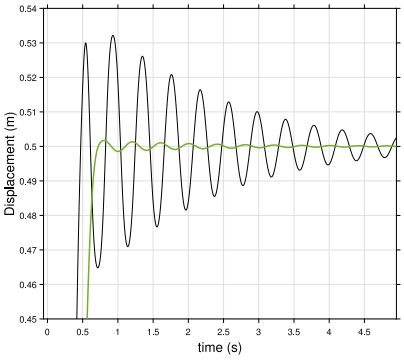
(c) Spectrum reference acc. $\ddot{r}(t)$



(d) Spectrum response θ



(e) Angle product $\theta(t)$



(f) Position product $x_2(t)$

Fig. 10. The time and frequency responses are shown both with the ZV input shaper (in green) and without it (in black). The reference trajectory 10(a) is 0.5 metres in 0.56 s and is shaped to a delay of 0.4 s, which is the vibration period of the swinging product. The corresponding maximum acceleration is 6.4 m/s^2 10(b). The acceleration spectrum after shaping 10(c) exhibits a frequency reduction at the resonance frequency of 2.5 Hz. The angle frequency spectrum shows suppression of the resonance peak at 2.5 Hz 10(d). The angle of the product shows a reduction in swing during motion and a rapid damping of the oscillations 10(e). In 10(f), it is demonstrated that the overshoot decreases from 30 mm to 1.7 mm, and the settling time, within a 5 mm range, is reduced from 1 to 4 s.

Table 2
Physical parameters delta robot.

Kinematic Parameters			Dynamic Parameters		
Sym.	Parameters	Value	Sym.	Parameters	Value
l_{1i}	Length Upper arm [mm]	348	m_{1i}	Mass Upper arm [kg]	0.949
l_{2i}	Length Forearm [mm]	800	m_{2i}	Mass Forearm [kg]	0.308
α_i	Offset rotary joints [mm]	200	m_2	Mass End-effector [kg]	0.026
β_i	Offset Travailing platform [mm]	45	m_1	Mass travailing platform [kg]	1.728



Fig. 11. The spider twin delta robot at the dynamics and control lab. Eindhoven University of Technology (TU/e). The high speeds and accelerations of this robot create a research environment to explore the trade-off between productivity and flexibility. Source Blue Print Automation [34].

5.2. Vacuum gripping and peel-off analysis

The current state-of-the-practice enclosure gripper designed for chicken fillets is complex and prone to maintenance problems. In addition, it requires spacing between the fillets for proper placement. Reviews in [2,35] address the handling of non-rigid food products and concluded that the handling of meat, poultry, and fish is particularly challenging. Choosing the gripper is crucial because using a dexterous hand brings unnecessary complications, and a contour-adapting gripper might damage the skin.

To address these challenges, research is conducted on the use of a flexible suction cup to handle picking and placing chicken fillets with varying weights. Peel-off is the process by which an object detaches from the vacuum gripper beneath it. The peeling force of vacuum grippers imposes limitations on the nominal acceleration during pick-and-place movements, affecting overall productivity. This limitation becomes evident during the horizontal movement of the product. Acceleration encounters resistance due to inertia, resulting in a lag in movement. This initiates vibrations in the product, exerting a considerable shear force on the vacuum gripper, which consequently loses its grip once the force surpasses the suction capacity. Figs. 14 and 15 illustrate this process for shaped and unshaped trajectories. During vertical motion in the pick-and-place cycle, the product is initially picked up at its centre of mass, resulting in minimal oscillation while moving upward. The horizontal movement begins at 0 s. In the acceleration phase, the product lags behind and is no longer centred under the end effector, causing a torque (shear force) on the vacuum gripper that peaks just after the reference acceleration switches to deceleration. This can result in a possible peel-off before the motion has concluded. The JL- and ZV-shaped trajectories, combined with adjusting the bandwidth

Table 3
Control parameters for input shapers and maximum acceleration obtained from the response measurements in the chicken fillet test for three pick positions. The fillet weight distribution and pick positions are depicted in Fig. 18.

Parameters/Pick position	1	2	3
Natural frequency [Hz]	1.40	1.43	1.38
Damping ratio [%]	7	5	14
Peel-off limit [m/s^2]	3.4	3.0	2.3

to match the oscillation frequency of the gripped object in the position joint controls (purple line), significantly reduce the load torque by more than three times. The ZV- and EI-shaped trajectories show reductions of approximately 2 and 3 times, respectively. During the downward motion, peel-off can happen if the picked object continues to swing and is not properly aligned under the bellow. This issue can be mitigated by input shaping, ensuring that when vibration occurs during the vertical downward direction, the object falls towards the intended placement position. In [36] a flexure based anthropomorphic gripper manufactured via metal additive technologies is reported. The flexture hinge framework has potential for a wide range of applications, while in combination with the optimisation procedure, superior designs can be obtained for tendon-driven grippers. To further enhance robustness against decentering and peel-detachment, a bellow vacuum gripper is augmented with a hinge mechanism, illustrated in Fig. 16a, a single rotational degree of freedom is added to an existing suction gripper. The design significantly reduces resistance against rotation due to the elastic and damping properties of the standard suction cup. In the model (13), (14), (15) and (16) the damping D_m and stiffness K_m are reduced to approach a free pendulum. Combining a rigid vacuum gripper with a hinge mechanism enables higher accelerations without the risk of peel-off, since the holding strength is not constrained by the vacuum gripper's spring force. The design shown in Fig. 16 is intended to be used alongside input shaping, ensuring that the gripper functions more like a pendulum. Fig. 17 illustrates the hinge gripper that holds a chicken fillet unpacked during a pick-and-place task. Tests with this prototype confirm that the hinge vacuum gripper can withstand a higher acceleration of 40% [37]. Because the small elastic suction component of the vacuum gripper stretches less, the sensitivity to variations in load mass and consequently the natural frequency ω_n are greatly diminished. This causes the gripped product to act similarly to a pendulum, resulting in more predictable oscillations and improved controllability. The transfer functions of the input shaper shown in Fig. 9 demonstrate a frequency dip in the area of the pendulum's natural oscillation for low damping ratios. Precise tuning minimises the overshoot when using the hinge vacuum gripper, due to its low damping characteristics.

5.3. The chicken fillet use case and its variations, a weight and pick-up spread case

The attributes of the chicken fillet scenario are outlined below:

(1) The flexible shape of the fillet leads to bending and swinging when picked and moved.
(2) Chicken fillets exhibit variations in weight and sizes, as depicted in Fig. 18a
(3) Variations in the pick location centre are present.
(4) Peel-off is not permitted.

The shape variation and the resulting centre of gravity lead to natural frequency variations of ±4%. The extensive weight distribution, ranging from 92 to 441 grammes, causes small ±5.5% variations in the natural frequency, ranging from 1.60 to 1.42 Hz. It is widely recognised that the ZV shaper is influenced by variations exceeding ten percent in vibration time due to changes in length when the mass is

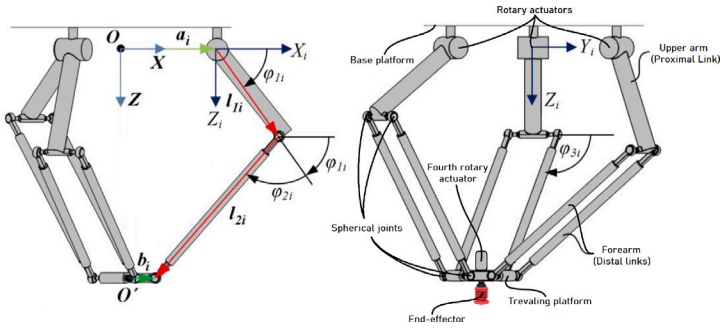
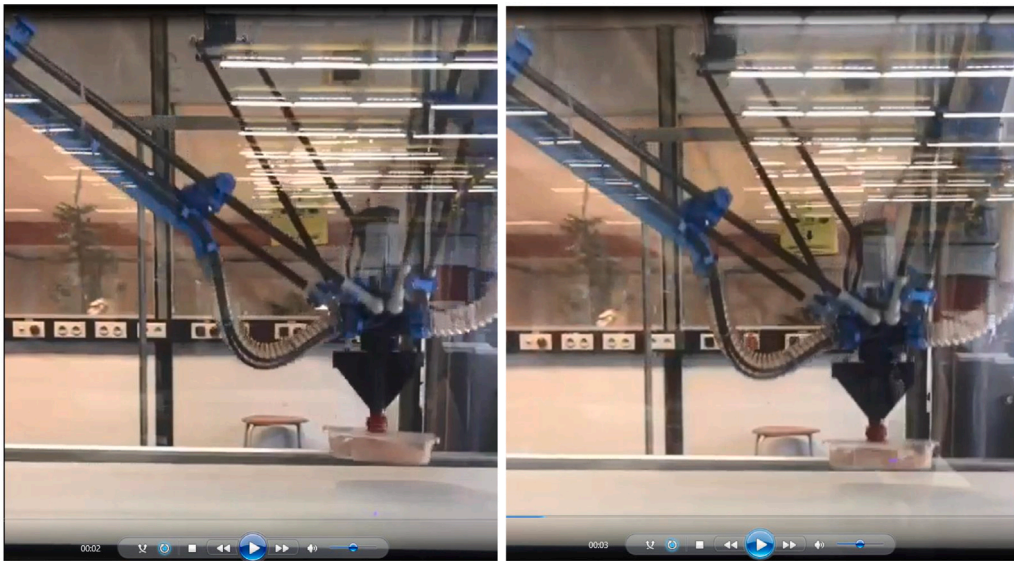


Fig. 12. Delta robot's mechanical design and its specifications, featuring a suction cup end effector at the bottom.



(a) Without input shaping (b) With input shaping

Fig. 13. Videos of a packed chicken fillet pick-and-place action with and without input shaping. Horizontal acceleration = 1.6 m/s^2 distance = 0.35 m move time = 0.48 s vibration time = 0.35 s τ = 0.75 s.

altered. In this case, the frequency range falls within this limit, and the ZV shaper effectively reduces the vibration. See also 9. The use of the ZV shaper can effectively handle these variations, limiting the overshoot to ensure the packing of all fillets and increasing the peel-off limit from 3 m/s^2 to 7 m/s^2. Table 3 presents the shaper parameters derived from the response measurements in a chicken fillet test carried out at various pick positions. Here, the peel-off limit is the maximum reference acceleration generated in the task space. Using the hinge gripper, this value can be increased to 40% as analysed in [37]. This is because the hinge gripper has reduced mechanical damping, allowing the input shaper to 'notch deeper' (see Fig. 9) and partly due to the closer resemblance to the pendulum model.

6. Automatic shaper parameter estimation for self tuning

Accurate values of the input shapers' parameters, obtained through measurements, are crucial, as the effectiveness of the feedforward method relies on the precise estimation of system parameters, specifically the natural frequency and damping ratio. The high-precision encoders located in the joints of the delta robot enable for rapid and precise estimation of parameters by using the sensitivity of position error signals affected by forces exerted on the end effector during swinging. These signals are read from one of three motion controllers, which predominantly operates in the direction of the swinging product. Fig. 19 shows the joint tracking errors observed during the 1-second movement period and the following settling phase. These subtle oscillations, distinctive for different products, enable the estimation of the system's natural frequency and damping ratio, as shown in Fig. 20 by subtracting the unloaded signal (the background) from the loaded one.

The damping ratio ζ can be derived through a second-order curve fit of the loaded tracking error minus the blank during the settling, representing the transient oscillation, as shown in Fig. 20b. Alternatively, it can be obtained using the equation:

$$\zeta = \frac{1}{2n\pi} \ln \frac{A_1}{A_n} \tag{21}$$

The number of swings equals n. A_n is the amplitude of the nth swing. To minimise the overshoot, it is beneficial to select low values of n because the vibration time is not constant and decreases during the settling

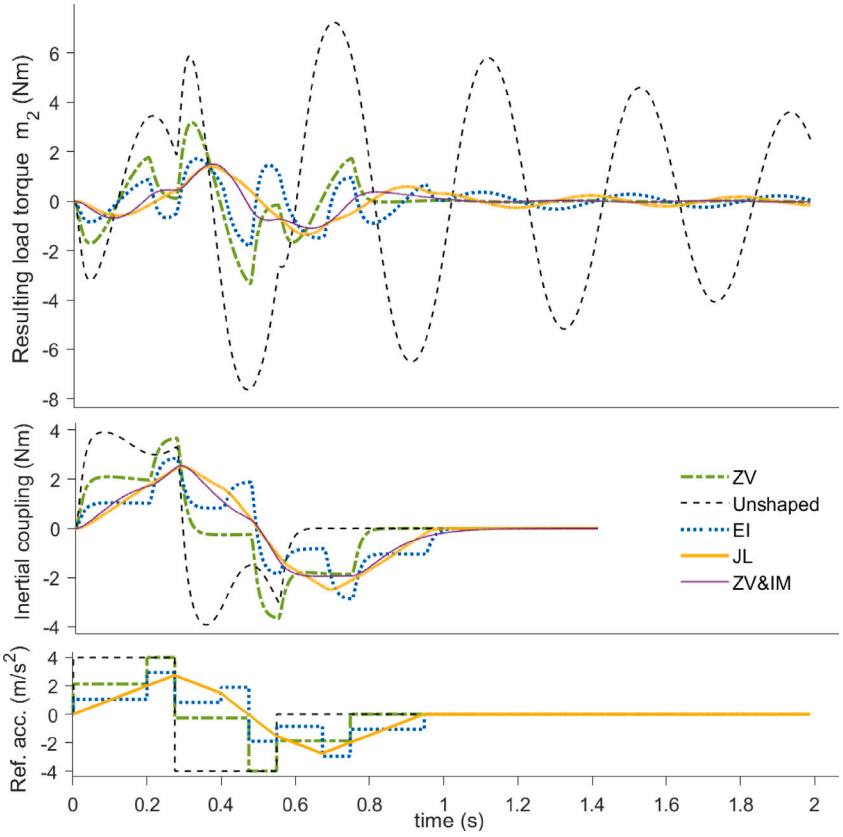


Fig. 14. Reduction of peel-off acceleration; Mass-cart-pendulum model simulation results for the resulting load torques exercised on mass m_2, the inertial coupling from end-effector to load mass m_2, the reference acceleration and the influence of input shapers. At $t = 0$, the product load m_2 is picked (end of the vertical upward motion), and the horizontal product transfer starts with high acceleration. At $t = 1$, the product is meant to be placed and the vertical downward motion starts.

process. The average time between zero crossings is used to determine the natural frequency. Self-tuning using the ZV input shaper can be successfully executed within three cycles of vibration. The estimated values obtained in the case of Fig. 20 are $\omega_n = 2\pi \cdot 0.51$ rad/s and $\zeta = 0.05$.

A broader approach involves utilising all three joint error signals and applying a coordinate transformation through the forward kinematic, rather than relying on signals from a single joint. When products exhibit significant differences, it is advisable to determine the natural frequency and damping during the initial phase of horizontal pick-and-place movement and subsequently apply them in the latter part of the move. Determining the damping ratio with high accuracy may not be feasible, as it requires several vibrations of the product. However, this parameter exerts the minimal impact on the input shaper's performance.

The move time delay introduced by input shaping results in synchronisation errors with other axes of the planned path. This issue can be addressed by either delaying the other trajectories or uniformly shaping all directions.

7. Conclusion

The dimensionless vibration time τ has a major influence on dynamic placement inaccuracy with and without the use of input shapers. Relations of the relative dynamic placement inaccuracy (overshoot) as a function τ have been derived for three relevant input shapers for robotic pick & place positioning of swinging products. Input shaping provides a significant reduction in overshoot, when the shaped move time is between 60% and 80% of the natural vibration time. Considering the allowable positioning inaccuracies and displacements, these curves can be employed to determine the minimum movement time.

For vertical length variations at pick-up up to 10%,corresponding to large weight variations, the ZV shaper provides the most effective suppression. When variations are between 10 and 20%, the ZV shaper achieves optimal performance if the bandwidth of the robot servo controllers is aligned with the system's vibration frequency.

To enhance robustness against decentering and peel-off, a hinge vacuum gripper has been designed, incorporating one rotational degree of freedom into a highly stiff bellow vacuum gripper. In a worst-case usage scenario test for chicken fillet packaging, this gripper with a ZV input shaper demonstrated significantly higher peel-off acceleration limits and vibration reduction for substantial variations in weight and pick locations, while maintaining oscillation frequency variations within $\pm 10\%$.

The controls have the capability of self-tuning by utilising the combined error signals in the delta robot systems through a background subtraction technique. This tuning proves to be effective within three oscillation cycles. It is crucial to distinctly separate trajectory generation intended to avoid actuator saturation from trajectories aimed at minimising vibrations. The proposed shaped trajectory is defined by displacement, move time, and maximum acceleration, intentionally bypassing the jerk and snap phases, which result in less optimal trajectories compared to the point-to-point movements discussed in this chapter. It is suggested for future research to investigate methods for automatically modifying shaper parameters during the second half of the first swing cycle, aiming to reduce the tuning duration.

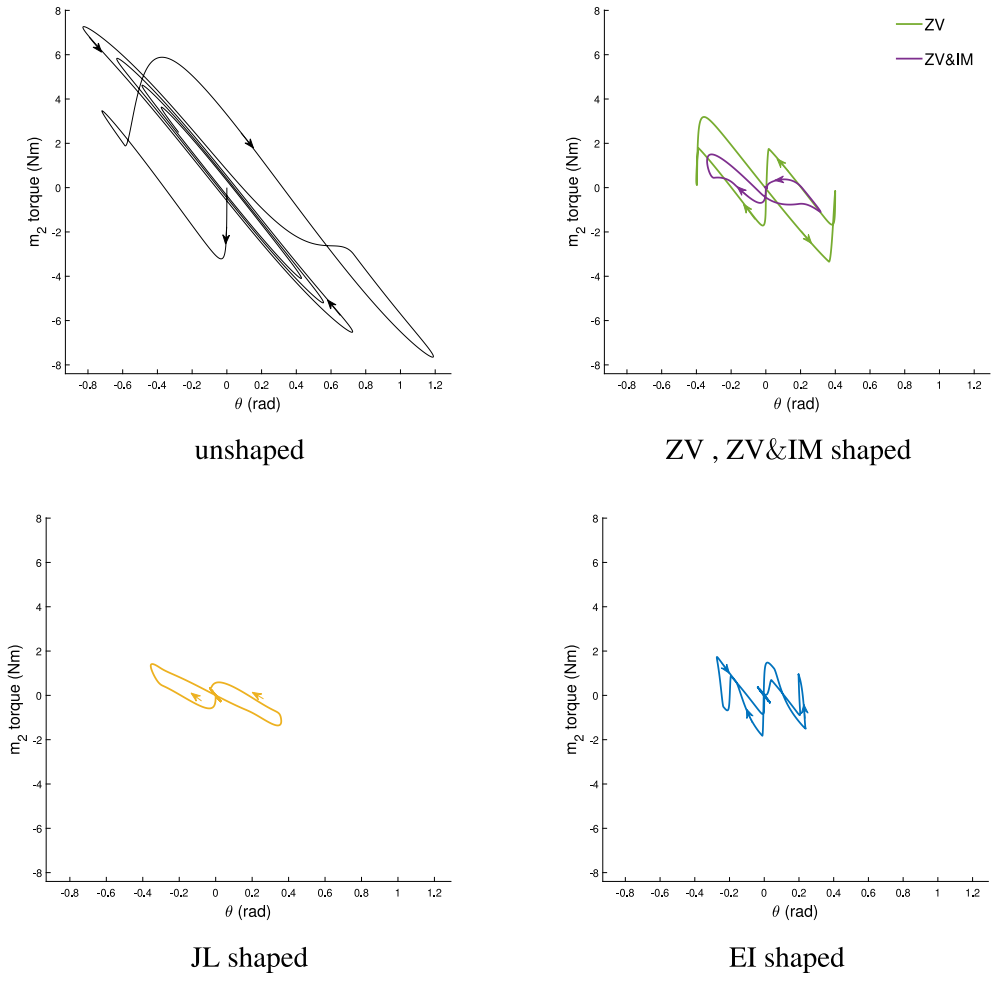
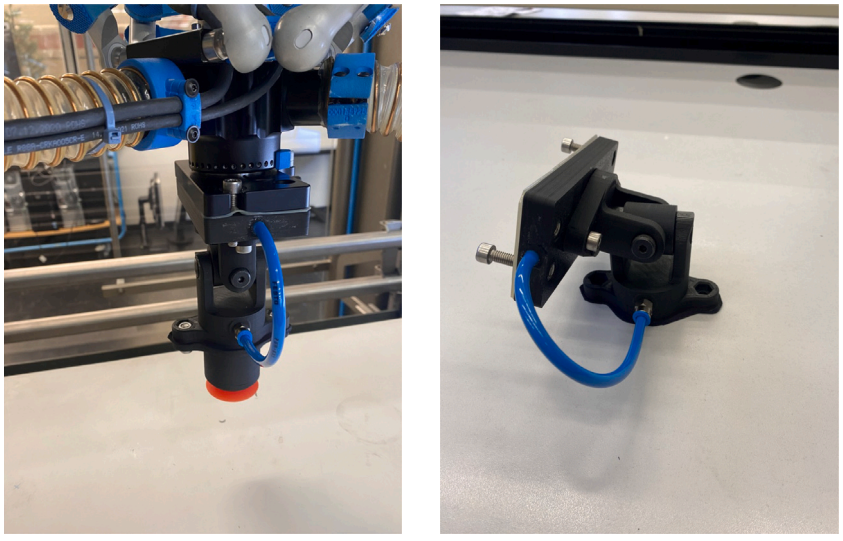


Fig. 15. Reduction of peel-off acceleration; Load torques at different values of the swinging angle θ during displacement of the pick-and-place movement. The shapers reduce both the swing angle and the resulting load torque. Nominal acceleration $a = 4$ m/s^2. The range of swing angles is $-0.8 < \theta < 1.2$ rad. Mass-cart-pendulum model.



(a) Single rotation hinge mounted to end-effector en suction cup (red).

(b) One axis hinge mechanism and interfaces to robot and bellow vacuum gripper.

Fig. 16. Construction of the hinge vacuum gripper which adds one rotational degree of freedom to the suction cup end-effector.

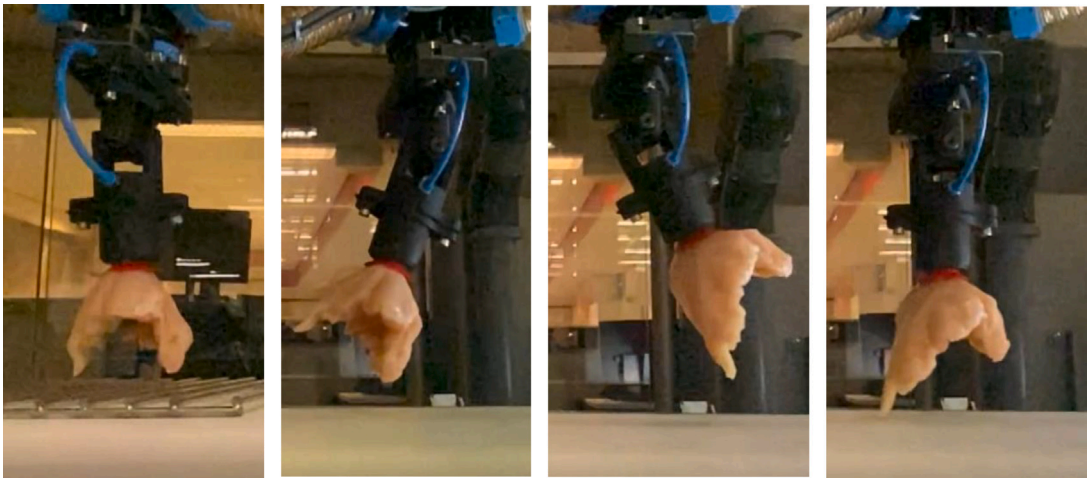
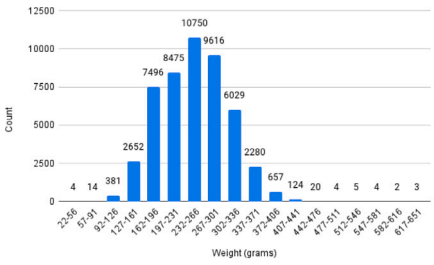
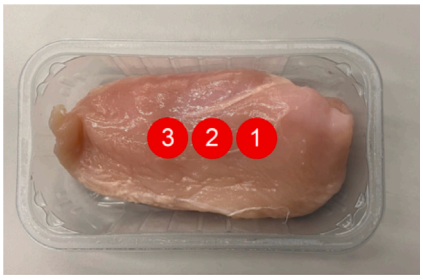


Fig. 17. Chicken fillet picked with hinge gripper (left) to reduce oscillations (middle) during placement (right).

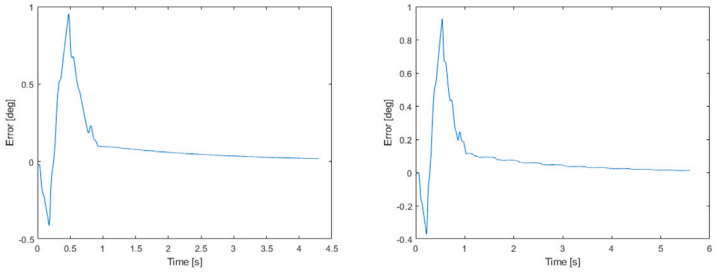


(a) Weight distribution of packaged chicken fillet product. Source Marel [4]



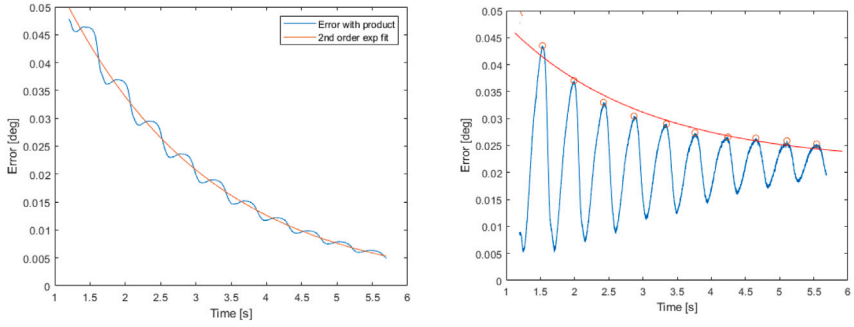
(b) Test sample for three pick positions.

Fig. 18. Packaged chicken fillet weight distribution and test sample pick up position label. The range is from 92 to 441 grammes.



(a) Background (no product load) (b) Tracking error when product is picked

Fig. 19. Joint tracking error signals during movement and settling in industrial motion controller. Measurements results with hinge gripper.



(a) Joint tracking error during settling and 2^{nd} order fit.

(b) Subtracted signal:
The transient oscillation and fitted damping

Fig. 20. Hinge gripper results after background subtraction to enable the fitted transient oscillation to deduce damped oscillation period T_d and damping ratio ζ.

CRediT authorship contribution statement

R.J. van der Kruk: Writing – review & editing, Writing – original draft, Software, Investigation, Formal analysis. **B.H.T. Bindels:** Validation, Software, Investigation. **H.P.J. Bruyninckx:** Writing – review & editing, Supervision, Funding acquisition. **M.J.G. van de Molengraft:** Supervision, Project administration, Funding acquisition.

Declaration of competing interest

The authors declare that they have no known competing financial interests or personal relationships that could have appeared to influence the work reported in this paper.

Acknowledgements

This research is supported by grants from the Netherlands Organisation for Scientific Research NWO/TTW in the Netherlands as part of the project Cognitive Robotics for Flexible Agro-Food Technology (FlexCRAFT).

Appendix A. Supplementary data

Supplementary material related to this article can be found online at https://doi.org/10.1016/j.robot.2024.104863.

Data availability

Data will be made available on request.

References

[1] Binay Kumar, Vacuum cup grippers for material handling in industry, Int. J. Innov. Sci. Eng. Technol. 4 (2017) 187–194.
[2] Zhongkui Wang, Shinichi Hirai, Sadao Kawamura, Challenges and opportunities in robotic food handling: A review, Front. Robot. AI 8 (2022).
[3] FooddrinkEurope, EU europe union food and drink retail figures 2023, 2024, (Accessed: 15 May 2024).
[4] Robbert van der Kruk, Arend Jan van Noorden, Tom Oomen, René van de Molengraft, Herman Bruyninckx, Robotic control for vibration reduction of swinging products, in: 2023 IEEE International Conference on Mechatronics, ICM, 2023, pp. 1–8.
[5] G.P. Starr, Swing-free transport of suspended objects with a robot manipulator, in: The 22nd IEEE Conference on Decision and Control, 1983, pp. 1484–1487.
[6] Marel, Food processing solutions, 2024, https://marel.com/. (Accessed: 02 October 2024).
[7] T. Glück, A. Eder, A. Kugi, Swing-up control of a triple pendulum on a cart with experimental validation, Automatica 49 (3) (2013) 801–808.
[8] Knut Graichen, Michael Treuer, Michael Zeitz, Swing-up of the double pendulum on a cart by feedforward and feedback control with experimental validation, Automatica 43 (1) (2007) 63–71.
[9] K.J. Aström, K. Furuta, Swinging up a pendulum by energy control, Automatica 36 (2) (2000) 287–295.
[10] N.C. Singer, W.P. Seering, Preshaping command inputs to reduce system vibration, J. Dyn. Syst. Meas. Control 112 (1) (1990) 76–82.
[11] Zaharuddin Mohamed, Jorge Martins, Mohammad Tokhi, Jenny da Costa, Miguel Ayala Botto, Vibration control of a very flexible manipulator system, Control Eng. Pract. 13 (2005) 267–277.
[12] William Singhose, Command shaping for flexible systems: A review of the first 50 years, Int. J. Precis. Eng. Manuf. 10 (4) (2009) 153–168.
[13] Khalid Alghanim, Abdulaziz Alfadhli, Asmahan Alshehemah, Abdullah Mohammed, Crane systems performance optimization through harmonic input shaper, Int. J. Dyn. Control (2023) 1–13.
[14] Nattapong Suksabai, Ittichote Chuckpaiwong, Input-shaped model reference control using sliding mode design for sway suppression of an industrial overhead crane, Eng. J. 27 (2) (2023) 1–15.
[15] Weiqiang Tang, Erpeng Zhao, Lijuan Sun, Haiyan Gao, An active swing suppression control scheme of overhead cranes based on input shaping model predictive control, Syst. Sci. Control Eng. 11 (1) (2023) 2188401.
[16] Mohammad Javad Maghsoudi, Z. Mohamed, S. Sudin, S. Buyamin, H.I. Jaafar, S.M. Ahmad, An improved input shaping design for an efficient sway control of a nonlinear 3D overhead crane with friction, Mech. Syst. Signal Process. 92 (2017) 364–378.
[17] Weiqiang Tang, Rui Ma, Wei Wang, Haiyan Gao, Optimization-based input-shaping swing control of overhead cranes, Appl. Sci. 13 (2023) 9637.
[18] H.I. Jaafar, Z. Mohamed, M.A. Shamsudin, N.A. Mohd Subha, Liyana Ramli, A.M. Abdullahi, Model reference command shaping for vibration control of multimode flexible systems with application to a double-pendulum overhead crane, Mech. Syst. Signal Process. 115 (2019) 677–695.
[19] William Singhose, Joshua Vaughan, Reducing vibration by digital filtering and input shaping, IEEE Trans. Control Syst. Technol. 19 (6) (2011) 1410–1420.
[20] Frank Boeren, Dennis Bruijnen, Niels van Dijk, Tom Oomen, Joint input shaping and feedforward for point-to-point motion : automated tuning for an industrial nanopositioning system, Mechatronics 24 (2014) 572–581.
[21] Tarunraj Singh, Optimal Reference Shaping for Dynamical Systems: Theory and Applications, CRC Press, 2010.
[22] Torsten Kröger, Friedrich M. Wahl, Online trajectory generation: Basic concepts for instantaneous reactions to unforeseen events, IEEE Trans. Robot. 26 (1) (2010) 94–111.
[23] Otto J.M. Smith, Posicast control of damped oscillatory systems, Proc. IRE 45 (9) (1957) 1249–1255.
[24] William Singhose, L. Pao, A comparison of input shaping and time-optimal flexible-body control, Control Eng. Pract. 5 (4) (1997) 459–467.
[25] Caglar Conker, Hakan Yavuz, Hasan Huseyin Bilgic, A review of command shaping techniques for elimination of residual vibrations in flexible-joint manipulators, J. Vibroeng. 18 (5) (2016) 2947–2958.
[26] Joshua Vaughan, Aika Yano, William Singhose, Comparison of robust input shapers, J. Sound Vib. 315 (4) (2008) 797–815.
[27] Pyung Hun Chang, Hyung-Soon Park, Time-varying input shaping technique applied to vibration reduction of an industrial robot, Control Eng. Pract. 13 (1) (2005) 121–130.
[28] Pu Zhao, Yunfei Zhou, Rougang Zhou, A new trajectory optimizing method using input shaping principles, Shock Vib. (2018).
[29] Ramón Piedrafita, Diego Comín, José Ramón Beltrán, Simulink® implementation and industrial test of input shaping techniques, Control Eng. Pract. 79 (2018) 1–21.
[30] B. Joseph, A tutorial on inferential control and its applications, in: Proceedings of the 1999 American Control Conference (Cat. No. 99CH36251), Vol. 5, 1999, pp. 3106–3118.
[31] Tom Oomen, Erik Grassens, Ferdinand Hendriks, Inferential motion control: Identification and robust control framework for positioning an unmeasurable point of interest, IEEE Trans. Control Syst. Technol. 23 (4) (2015) 1602–1610.
[32] Mark W. Noakes, John F. Jansen, Generalized inputs for damped-vibration control of suspended payloads, Robot. Auton. Syst. 10 (2) (1992) 199–205.
[33] Gürsel Alici, Sadettin Kapucu, Sedat Bayseç, Swing-free transportation of suspended objects with robot manipulators, Robotica 17 (5) (1999) 513–521.
[34] Blueprint Automation, BluePrint automation, 2024, 02/10/2024. https://blueprintautomation.com/en/.
[35] P.Y. Chua, T. Ilschner, D.G. Caldwell, Robotic manipulation of food products – a review, Ind. Robot: Int. J. (2003).
[36] Martin Tschiersky, Jan J. de Jong, Dannis M. Brouwer, Flexure hinge design and optimization for compact anthropomorphic grippers made via metal additive manufacturing, J. Mech. Des. 146 (1) (2023) 015001.
[37] B.H.T Bindels, Towards Automatic Control of Swinging Flexible Food Products in Pick-And-Place Applications, Technical University of Eindhoven, 2023.



Robbert van der Kruk During the research described in this article, Robbert van der Kruk is a senior academic researcher in the Control Systems Technology group at Eindhoven University of Technology (TU/e) in Eindhoven (NL). He is a former R&D manager at Philips, ASML and Agilent Technologies. He is pursuing a Ph.D.